COMPARATIVE MODELING OF PLASMA BOUNDARY CORRUGATION DUE TO THE APPLICATION OF 3-D FIELDS WITH ELM CONTROL COILS IN VARIOUS ITER SCENARIOS

L. LI, F. C. ZHONG
College of Science, Donghua University
Shanghai 201620, China
Email: lili8068@dhu.edu.cn

Y.Q. LIU
General Atomics
PO Box 85608, San Diego, CA 92186-5608, USA

A. LOARTE, S. D. PINCHES, A. R. POLEVOI
ITER Organization
Route de Vinon-sur-Verdon, CS 90046, St Paul-lez-Durance Cedex,France

Abstract

For the purpose of better understanding the type-I ELM control in ITER with RMP fields, the plasma response to RMP is computed based on a resistive full magneto-hydrodynamic model in toroidal geometry. Five scenarios designed for ITER are considered ranging from the pre-nuclear to nuclear phases. The plasma response to RMP is quantified by the plasma surface displacement near the X-point and the outboard mid-plane. The optimal coil configurations between the two high Q DT scenarios (same plasma current 15 MA and same magnetic field 5.3 T but different fusion gains, Q=5 and 10, corresponding to different operating densities, respectively) are similar. For the other ITER scenarios with similar q_{95} to the baseline (q_{95}~3), the optimal coil phasing is also similar. The exception is the half-current full-field (7.5 MA/ 5.3 T) scenario, which significantly differs due to the much higher q_{95}. The RMP coil currents are also optimized to tailor the core versus edge toroidal torques, exerted by the 3D fields on the plasma column. The torque optimization, with various objective functions proposed in the study, can be useful, for instance, to minimize the RMP effect on the plasma flow in ITER, whilst still maintaining the ELM control capability.

1. INTRODUCTION

Large scale edge localized modes (ELMs), the so called type-I ELMs, often lead to a substantial amount of particles and energy being released from the plasma into the plasma facing components (PFCs). This can significantly increase the erosion rates of PFCs and reduce their lifetime to unacceptable levels for reliable ITER operation [1]. Application of 3D external resonant magnetic perturbation (RMP) fields has been experimentally demonstrated to provide successful suppression or mitigation of type-I ELMs in many tokamaks [2-8]. Extensive theory and modeling work has been carried out to understand ELM control physics with RMP fields, although the understanding is still far from complete. Nevertheless, it has been widely recognized that the plasma response plays an important role in ELM control [9-12]. Previous work [13-16] has shown that the normal displacement of the plasma surface, or in other words the 3D corrugation of plasma boundary, caused by RMP fields and computed by MHD codes such as MARS-F [17], can be used as a reliable indicator to describe global features of the plasma response and the resulting transport properties that affect the behavior of ELMs.

In this paper, we investigate the plasma displacement caused by RMP fields for five representative ITER plasma scenarios, ranging from the initial H-mode operation in PFPO phase to the Q = 10 DT operation in FPO. The computed plasma surface corrugation is used as a proxy to understand the capability and robustness of the type-I ELM control in ITER in these various plasma scenarios. The consider plasma scenarios cover the plasma current range of 5-7.5-15 MA, with the magnetic field varied in proportion such that q_{95} ~ 3 is fixed, as well as a case with q_{95} ~ 6 at 7.5 MA current. Besides the direct relevance of the computed plasma surface corrugation to ELM control as reported in this work, the full database (the plasma displacement and the magnetic field perturbations due to the plasma response) from this systematic ITER investigation also serves an essential input to further studies, such as the divertor power flux assessment in the presence of RMP fields.

Furthermore, 3D RMP fields also produce toroidal torques as a result of the plasma response. These torques can modify the toroidal plasma flow, potentially leading to rotation braking. This may be a concern for ITER, considering the expected moderate flow speed in ITER plasmas due to the low (normalized) input torque provided by the negative neutral beams.. A self-consistent investigation of the flow damping requires at least

quasi-linear initial value simulations. In this work, however, we adopt another approach. We study the toroidal torque profiles computed from linear response modelling, and optimize these radial profiles by varying the RMP coil currents, according to various criteria.

2. VARIOUS ITER SCENARIOS AND COMPUTATIONAL MODEL

The ITER Research Plan defines the development path of ITER operational scenarios from First Plasma to the achievement of the ITER fusion power production goals with two main phases: Pre-Fusion Power Operation (PFPO) phase (with two sub-phases PFPO-I and PFPO-II) and the Fusion Power Operation (PFO) phase. Five representative ITER plasmas are considered in our studies to cover the H-mode operation in these phases up to the achievement of the Q = 10 fusion power goal. The key parameters of these five H-mode plasmas are listed in table 1. The PFPO-1 phase (case 1) is the first stage in ITER operation after first plasma, exploring Radiofrequency (RF) heated hydrogen/helium plasma discharges. The plasma current for these RF heated H-mode plasmas I_p is 5 MA and the toroidal magnetic field B_T is 1.8 T, which are both 1/3 of those of the Q = 10 baseline scenario (15 MA/5.3 T). To study the ELM control issues in the expansion of the H-mode operational space towards the final 15 MA/5.3T to be performed partly in PFPO-II and in FPO, two cases are considered both with the same plasma current (7.5 MA) but different toroidal magnetic field (half-field of 2.65 T for case 2 and full-field of 5.3 T for case 3). For 15 MA/5.3T high Q operation two H-mode plasmas are considered with two levels of plasma density providing Q = 5 and Q =10 respectively (case 4 and case 5). Therefore, except case 3 (7.5 MA/5.3 T), all the others plasmas have similar edge safety factor q_{95} (~ 3) as shown in table 1. Figure 1 compares the radial profiles of the equilibrium pressure and safety factor of all five ITER H-mode plasmas studied.

TABLE 1. SUMMARY OF THE FIVE ITER SCENARIOS.

Case No.	$I_p/B_T/Q$	q_0	q_{95}	β_N
1	5 MA/1.8 T	0.96	3.12	1.07
2	7.5 MA/2.65 T	1.28	3.17	2.08
3	7.5 MA/5.3 T	0.96	6.17	1.38
4	15 MA/5.3 T/5	1.07	3.13	1.46
5	15 MA/5.3 T/10	1.01	3.14	1.97

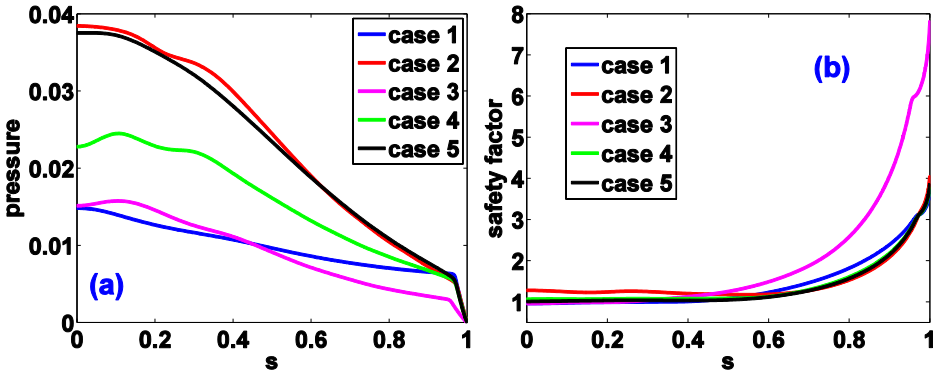

FIG. 1. Comparison of radial profiles of (a) equilibrium pressure (normalized by B_0^2/μ_0) and (b) safety fator, between all five ITER scenarios shown in table 1.

The plasma toroidal flow generally affects the plasma response to RMP fields. In this work, the toroidal flow profiles for these ITER scenarios are self-consistently calculated by the transport code ASTRA. The code predicts the rotation profiles including the NBI momentum input, as well as assuming two key parameters - the Prandtl number (P_r) and the ratio of the toroidal momentum to thermal confinement times (τ_Φ/τ_E). For the same ITER scenario, various flow profiles are obtained by ASTRA, depending on the choice of values for the aforementioned momentum transport coefficients. For the PFPO-1 plasma (with no NBI) a range of rotation profiles are considered to account for a range of intrinsic rotation levels, with the upper level considered as that corresponding to the rotation of the plasma if it were heated by 10 MW of NBI which corresponds to a high

level of intrinsic rotation. It is important to note that the MARS-F computations show certain degree of robustness of the plasma response against the variation of flow for these ITER plasmas (to be reported elsewhere). In this work, we focus on reporting MARS-F results at fixed values of Pr=0.3 and τ_Φ/τ_E =2.

The ITER baseline design includes 27 ELM control coils, located at the outside of the plasma torus and divided into three toroidal rows (9 coils per row). In total 27 independent power supplies will be available for the ITER operation beyond PFPO-II (e.g. for cases 2-5 shown in table 1), in order to drive the ELM control coil currents. However, only a fraction of power supplies (~ 9 supplies) are been presently considered for the initial PFPO-I phase (case 1 from table 1).

The MARS-F code [17] solves the single fluid, linearized resistive magneto-hydrodynamic (MHD) equations in toroidal geometry. The RMP coil currents are treated as source terms in the code. Following previous work [13-16], the plasma surface displacements near the X-point and at the outboard mid-plane, as well as their ratio, are three critical parameters used to describe the plasma boundary corrugation. These figures of merit are under systematic investigation for various ITER scenarios.

3. NUMERICAL RESULTS

In what follows, we compute and compare the linear (i.e. plasma displacement) and quadratic (i.e. toroidal torques) response of the five ITER plasmas described in the previous section. For the linear response study, we fix the RMP coil current amplitude at 1 kAt.

3.1. Comparison of plasma surface displacement between various ITER scenarios

We first compare the MARS-F computed plasma surface displacement between various cases. The plasma toroidal rotation frequencies, shown in Fig. 2(a), were obtained assuming the same momentum transport parameters (Pr=0.3 and τ_Φ/τ_E =2). The plasma surface displacement, caused by the upper, middle, and lower rows of coils individually, is compared in plots (b-d), respectively. Note that, given the same RMP coil current, the displacement amplitude is normalized by the corresponding plasma current for different scenarios. We remark that this is a reasonable but not unique way of normalizing (and thus comparing) the plasma response between different scenarios.

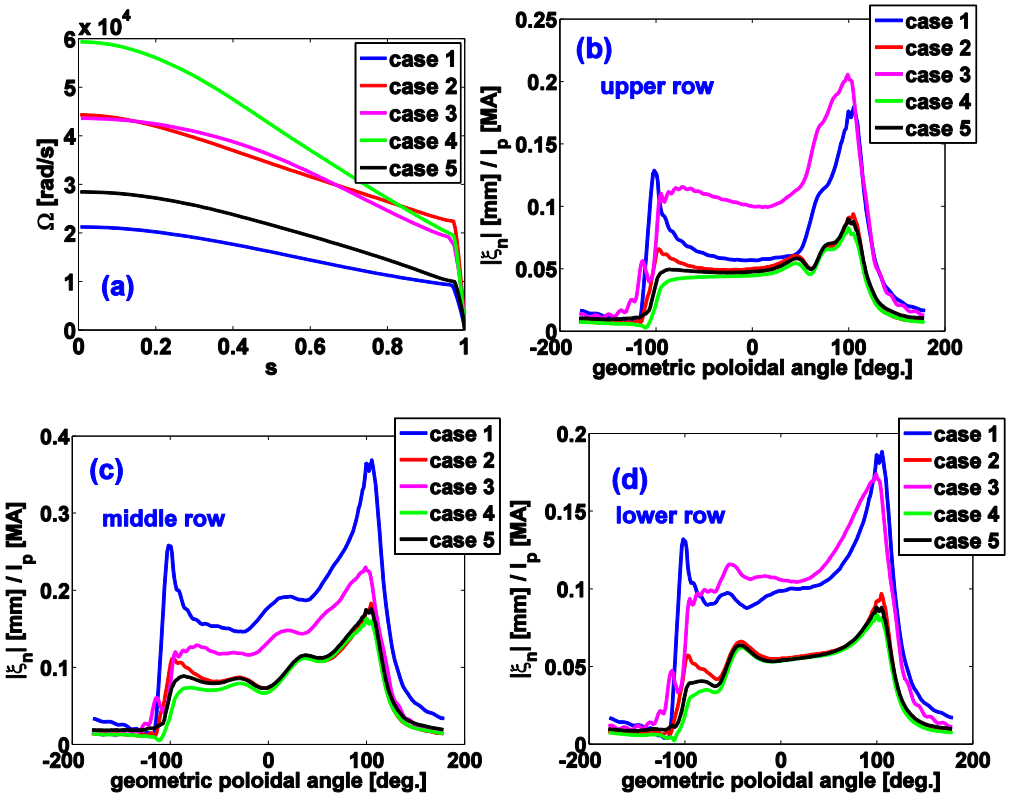

FIG. 2. (a) Comparison of radial profiles of the toroidal rotation frequency, which is predicted by the ASTRA with same transport model (P_r=0.3, τ_φ/τ_E=2). Comparison of the plasma surface displacement along the poloidal angle for different ITER plasmas (denoted by different colors), produced by (b) the upper row of coil current, (c) the middle row, and (d) the lower row. Here, the plasma surface displacement (in mm) is normalized by the total plasma current I_p (in MA), a maximum 1 kAt coil current and a sinosoidal n = 3 waveform is assumed for each row.

Several interesting observations can be made. First, the plasma response between the two high Q plasmas (case 4 and case 5) is similar for all three rows of coils, despite the fact that the equilibrium pressure (Fig. 1(a)) and the plasma flow frequency (Fig. 2(a)) are different. The key reason for the close response between these two cases is an almost identical radial profile of the safety factor as shown in Fig. 1(b). The plasma pressure (β_N shown in table 1) is still well below the Troyon no-wall limit, and hence the pressure effect on the plasma response is not significant [18]. The nearly factor of two difference in the plasma toroidal flow does not affect much the response either. This agrees with the previous findings [19, 20], that the plasma response is not very sensitive to the flow amplitude variation, unless the latter varies by an order of magnitude. In the following study, we choose the Q = 10 scenario (case 5) as the representative one for 15 MA/5.3T plasmas.

Next, we compare the plasma response between case 3 (7.5 MA/5.3 T) and case 5 (15 MA/5.3 T). These two cases have the same magnetic field but different plasma current, resulting in different q_{95} (Fig. 1(b)). The computed plasma response between these two cases is rather different. The difference largely comes from the safety factor, as shown in previous work [15, 16]. This should lead to different results in ELM control if the same RMP coil current level and waveforms are applied for these two plasmas.

Finally, it is interesting to compare the plasma response between the three ITER plasmas with similar q_{95}, i.e. case 1 (5 MA/1.8 T denoted by blue lines), case 2 (7.5 MA/2.65 T denoted by red lines), and case 5 (15 MA/5.3 T denoted by black lines). The normal surface displacement is similar between cases 2 and 5, after the normalization by I_p. The plasma response in case 1 is the largest among these three cases. This may be related to the slowest pedestal plasma flow in case 1. The overall shapes (without considering the magnitude) of the displacement curves, on the other hand, remain similar among these three ITER scenarios with similar q_{95}.

3.2. Optimization of ELM control for various ITER scenarios based on plasma surface displacement

Here we optimize the ELM control coil currents for the five ITER scenarios, using criteria based on the MARS-F computed plasma surface displacement. For a given toroidal mode number n, we denote the RMP coil currents by $I_U\exp(in\Phi_U)$, $I_M\exp(in\Phi_M)$ and $I_L\exp(in\Phi_L)$, for the upper, middle and lower rows, respectively.

According to Refs. [13-16], a better ELM control is achieved, if the applied vacuum RMP field spectrum maximizes the edge-peeling component in the plasma response, which in turn is manifested by the large plasma surface displacement near the X-point $|\xi_X|$. The opposite limit maximizes the core-kink response of the plasma, leading to large plasma displacement near the outboard mid-plane $|\xi_M|$. Our strategy is therefore to maximize $|\xi_X|$ while minimize $|\xi_M|$. Since it often occurs that a minimal $|\xi_M|$ value of near 0 can be achieved in multi-dimensional parameter space, we avoid this situation by designing an objective function (OF) as $|\xi_X|/max(\alpha|\xi_M^{max}|,\ |\xi_M|)$, where α is a weighting factor. The choice of α dictates a lower bound for the mid-plane displacement, that we wish to minimize. A systematic scan of the α-value, between 0 and 1, and the subsequent investigation of the robustness of the optima, indicates that α=0.5 is a reasonable choice. This result in optimal coil phasing that is not far from maximizing the plasma boundary displacement near the X-point, meanwhile keeping mid-plane displacement $|\xi_M|$ well bounded from below.

As an example, Fig. 3 reports the optimization results for the scenario with 15 MA/5.3 T plasma at Q=10. Considered are three combinations of the coil rows in the n=3 configuration: the middle row alone (blue dashed lines in the upper panel), two off-middle rows (red solid lines in the upper panel) and all three rows (bottom panel). The full coil phasing scans are performed, while recording plasma displacement near the X-point (left panel), at the outboard mid-plane (middle panel), and their ratio according to the above definition (OF with α=0.5, right panel). If only the two off-middle rows are used for ELM control, the peak value of OF is achieved at the coil phasing of Φ_U-Φ_L =66^o. This peak value is similar to that of the middle row alone, but achieved at reduced mid-place displacement. Similar effect is achieved with three rows of coils. The peak value of OF in this case is achieved at Φ_U-Φ_M =170^o, Φ_L-Φ_M =235^o. Note that coil phasing is different from the one that maximizes the X-point displacement (200^o, 140^o) or the one that minimizes the outboard mid-plane displacement (95^o, 275^o). Given the similarity of the overall patterns between the X-point and the mid-plane

displacements, indicating the strong coupling between these two types of plasma response as long as the coil phasing optimization is concerned, our definition of the OF helps to reduce this coupling effect.

Note also that, with inclusion of all three rows, the optimization in the 2D parameter space leads to a somewhat higher value of OF, as compared to that using single row or two off-midplane rows, and a larger X-point displacement at the optimum OF. This is evidence of the fact that three rows of coils offer more flexibility in choosing the coil phasing for the ELM control in ITER.

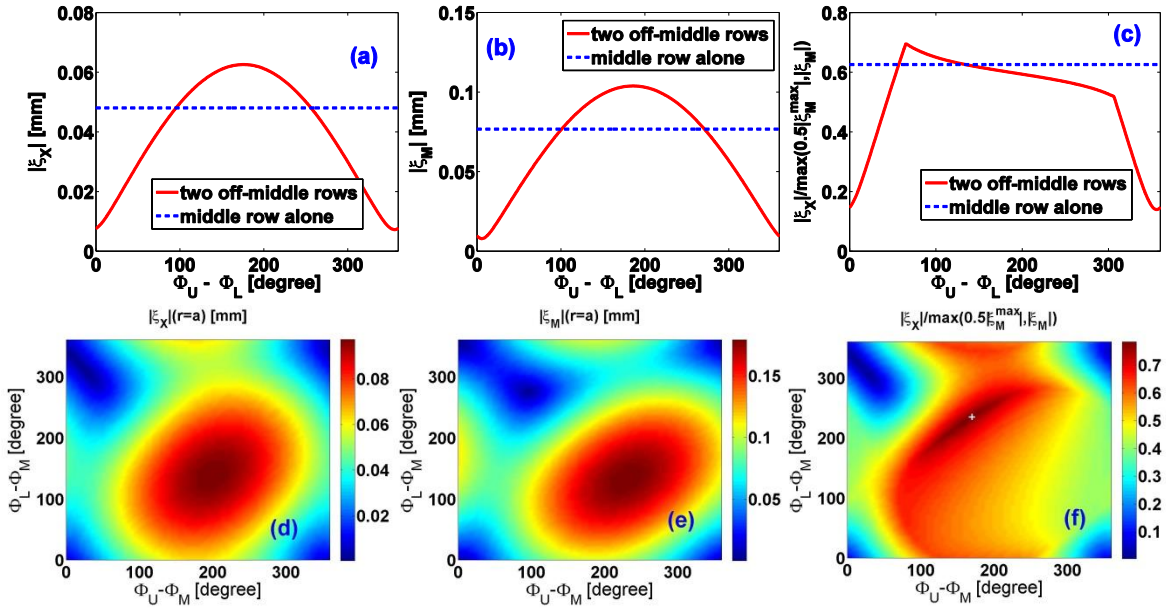

FIG. 3. Comparison of the n=3 plasma surface displacement near the X-point (left panels), at the outboard mid-plane (middle panels), and the value of OF $|\xi_X|/max(\alpha|\xi_M^{max}|,\ |\xi_M|)$ *(right panels), between the single middle row (upper panels, dashed lines), two off-middle row (upper panels, solid lines), and three-row (lower panels) coil configurations, for the full-current full-field ITER baseline DT plasma at Q=10 (case 5 from table 1). Relative coil phasing between different rows is scanned for the two-row and three-row configurations. The coil current amplitude is assumed to be 1 kAt and n=3 toroidal symmetry is used (note that the maximum ELM control coil current is 90 kAt). Toroidal plasma rotation is modeled by ASTRA assuming Pr=0.3,* τ_ϕ/τ_e*=2.*

Similar studies are also performed for all five ITER plasmas using the n=3 configuration. Since the plasma current (and hence the equilibrium poloidal field) varies within these scenarios, we fix the ratio of the coil current amplitude to the plasma current at I_{RMP} [kAt]/I_p [MA] = 1/15. Thus, the coil current is 1 kAt for the 15 MA plasmas, but will be 0.5 kAt for the 7.5 MA plasma. The plasma flow is again obtained assuming Pr=0.3 and τ_ϕ/τ_e=2 in all cases.

Note that, for cases 2-5, the availability of 27 independent power supplies enables a continuous coil phasing scan between three rows. Sinusoidal waveform of the coil current distribution along the toroidal angle is used for each row. For case 1 (the 5 MA/1.8 T scenario in PFPO-I), however, we assume that only a restricted set of power supplies is available. We have to use piece-wise constant waveforms for the coil current distribution, for instance '+1 -1 0 +1 -1 0 +1 -1 0' or '+0.5 +0.5 -1 +0.5 +0.5 -1 +0.5 +0.5 -1' (note that these current distributions ensure vanishing net current along the toroidal angle). These piece-wise constant waveforms lead to discrete values for the choice of the coil phasing, in fact with an incremental factor of 60°.

With the above considerations, in table 2 we report and compare the coil phasing optimization results for all five scenarios and using all three rows of coils. Generally speaking, the optimal coil phasing, based on maximizing the plasma surface displacement near the X-point while minimizing the mid-plane displacement, is similar for scenarios with similar q_{95}. The scenario with different q_{95} (i.e. case 3 with 7.5 MA/ 5.3 T) has different optima. In addition, since case 1 (5 MA/1.8 T) has limited available choices for the coil phasing, the optima deviates somewhat from those of the other three cases (cases 2, 4 and 5).

TABLE 2. OPTIMIZATION RESULTS WITH THREE ROWS OF ELM CONTROL COILS FOR CASE 1-5, ASSUMING THE N=3 COIL CONFIGURATION, WITH FIXED COIL CURRENT AMPLITUDE AT I_{RMP} [kAt]/I_p [MA] = 1/15. CASE 2-5 ASSUME 27 POWER SUPPLIES, WHILST CASE 1 ASSUMES A RESTRICTED SET OF POWER SUPPLIES.

Case	Φ_U-Φ_M	Φ_L-Φ_M	Max|ξ_X| [mm]	Φ_U-Φ_M	Φ_L-Φ_M	Min|ξ_M| [mm]	Φ_U-Φ_M	Φ_L-Φ_M	Max OF-value
1	240 ^{O}	120 ^{O}	0.169	60 ^{O}	300 ^{O}	0.0040	180 ^{O}	360 ^{O}	1.965
2	190 ^{O}	145 ^{O}	0.157	90 ^{O}	275 ^{O}	0.0015	155 ^{O}	230 ^{O}	1.304
3	330 ^{O}	20 ^{O}	0.134	115 ^{O}	265 ^{O}	0.0014	255 ^{O}	255 ^{O}	0.490
4	210 ^{O}	130 ^{O}	0.053	10 ^{O}	350 ^{O}	0.0008	170 ^{O}	225 ^{O}	0.415
5	200 ^{O}	140 ^{O}	0.097	95 ^{O}	275 ^{O}	0.0001	170 ^{O}	235 ^{O}	0.782

3.3. Optimization of toroidal torque profiles produced by 3D RMP fields

In this sub-section, we shall focus on tailoring the radial profiles of the toroidal torque profiles for ITER, by varying the poloidal spectrum of the applied RMP fields. More specifically, we maximize or minimize torque amplitude in the plasma core relative to that in the edge region. We focus on case 5 with 15 MA/5.3 T and Q=10, and with the n=3 coil configuration. The plasma flow is again obtained by ASTRA assuming Pr=0.3 and τ_Φ/τ_E =2. Here, the toroidal torques computed by the MARS-F code include the NTV torque, the *j*x*b* torque associated with the Maxwell stress tensor and the torque due to the Reynolds stress. For the optimization study, we consider the total torque density contributed by all three torques.

The torque profile optimization is carried out by varying the coil current amplitude and phase in three rows of RMP coils. We design several objective functions (OFs). For the purpose of ELM control, we may wish to maximize the edge flow damping in order to allow better penetration of the applied 3D field. Meanwhile, we may also wish to minimize the side effect of the RMP field on the core flow damping. This dictates the optimization strategy of maximizing the toroidal torque near the plasma edge whilst minimizing the one in the core plasma. The corresponding objective functions will be denoted as 'OF*A'. On the contrary, the OFs that minimize the edge torque while maximizing the core torque (the 'worst' solution for ELM control in ITER) will be denoted as 'OF*B'. In order to definite the core and edge torque density, we divide the plasma region into tow sub-regions: the core plasma region with minor radius s=(0, 0.89) and the edge plasma region with s=(0.89, 0.995). The reason for this division is to include the pedestal region into the edge region. The torque contribution outside the s=0.995 surface is ignored, for the sake of achieving numerical robustness of the results.

At each radial location s, the total torque density, with a given set of three-row coil currents $X = [A_U \ A_M \ A_L]^T$, can be obtained via a quadratic form $T_{tot}(s) = Re[X^T \Pi_{tot} X^*]$, where Π_{tot} is a total torque density matrix computed by MARS-F. We further define

$$T_{core} = \max|T_{tot}(s)|, \quad 0 < s < 0.89,$$
$$T_{edge} = \max|T_{tot}(s)|, \quad 0.89 < s < 0.995.$$

Based on T_{core} and T_{edge}, we design four OFs,

OF1A: $\min(T_{core})$,
OF2A: $\max(T_{edge})$,
OF3A: $\min(T_{core}/T_{edge})$,

The corresponding 'opposite' OFs are, respectively,

OF1B: $\max(T_{core})$,
OF2B: $\min(T_{edge})$,
OF3B: $\max(T_{core}/T_{edge})$.

A global optimization in 5D parameter space $(\Phi_U - \Phi_M, \Phi_L - \Phi_M, I_U, I_M, I_L)$ is computed with the constraint that three rows of coil current add up to 90 kAt. The constraint on the coil current amplitude effectively renders this to a 4D space optimization. The optimal solutions are collected in Table 3. The optimal torque density profiles are plotted in Fig. 4, using various OFs.

In general, the optimal torque density profiles confirm a trend, that the core and the edge torques couple to each other. This can be observed in the overall pictures plotted in Fig. 4 as well as the optimal coil current solutions

reported in table 3. For instance, maximizing the edge torque (OF2A) and maximizing the core torque (OF1B) both result in the same optimal point – using maximum current in the middle-row coils only. On the other hand, the objective function OF3 helps to decouple the core torque from the edge. Secondly, the overall torque density amplitude across the whole plasma column can differ by orders of magnitude, depending on the choice of objective functions. There is no unique way of deciding which is the 'best' OF to be chosen. If we wish to maximize the edge/core torque ratio and at the same time have the least impact on the whole plasma flow, the OF3A appears to be the best choice. But, if the edge torque is not sufficiently large to brake the flow in the pedestal region and to allow the RMP field penetration, we may need to choose OF2A to obtain a larger edge torque (but meanwhile with the potential danger of braking the core flow as well).

TABLE 3. SUMMARY OF ALL OPTIMAL RMP COIL CONFIGURATIONS, ASSUMING FOUR OBJECTIVE FUNCTIONS IN 5D SPACE. THE SUM OF MAXIMUM CURRENT IN THE THREE ROWS OF COIL CURRENT AMPLITUDE IS FIXED AS 90 KAT.

Objective function	Phase [deg.]		Amplitude [kAt] $I_U+I_M+I_L$=90 kAt			T_{core} [N/m^2]	T_{edge} [N/m^2]
	Φ_U-Φ_M	Φ_L-Φ_M	I_U	I_M	I_L		
OF1A: min(T_{core})	289	330	28.6	16.4	45.0	4.8566e-03	9.3191e-01
OF2A: max(T_{edge})	-	-	0	90	0	3.6732e+00	6.3792e+01
OF3A:min(T_{core}/T_{edge})	279	324	32.7	12.2	45.1	5.3811e-03	1.6158e+00
OF1B: max(T_{core})	-	-	0	90	0	3.6732e+00	6.3792e+01
OF2B: min(T_{edge})	304	5	32.7	14.3	43.0	6.0646e-02	3.5190e-01
OF3B: max(T_{core}/T_{edge})	213	309	40.9	4.1	45.0	1.6626e-01	5.3157e-01

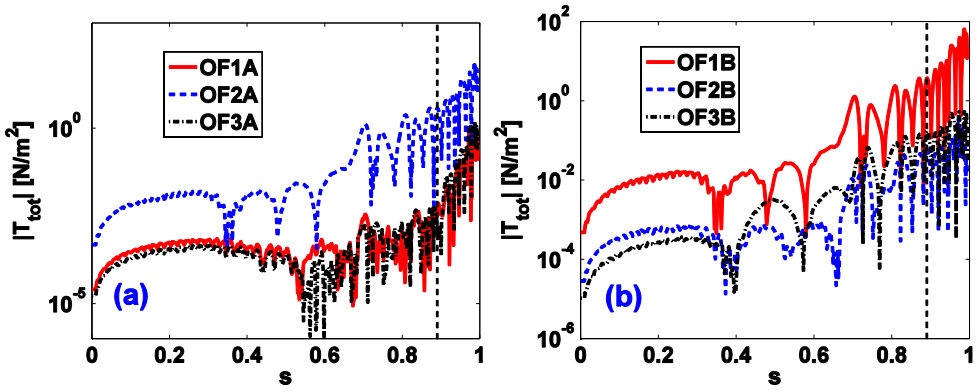

FIG. 4. Comparison of the absolute value of the torque density amplitude according to different objective functions, where (a) comparison of the 'best' and (b) the 'opposite' torque profiles according to OF1-3. The corresponding optimal RMP coil configurations are reported in table 3.

4. CONCLUSION

In summary, based on the 3D plasma surface displacement produced by the fields produced by the ELM control coils, we have numerically investigated the plasma response in five ITER scenarios with the full set of 27 power supplies for PFPO-II and FPO and a restricted set of power supplies for PFPO-I, in order to understand the robustness of the type-I ELM control in ITER using RMP fields. It is found that, the plasma surface displacement is similar between the two high Q scenarios with the same plasma current (15 MA) and magnetic field (5.3 T) but with different fusion gain (Q=5 and 10) due to different operating density. For these ITER scenarios, the plasma response amplitude (normalized by the equilibrium plasma current) is largely dictated by q_{95}.

Optimization of the ELM control current waveform phasing in 2D space (Φ_U-Φ_M, Φ_L-Φ_M) for all five H-mode plasmas, has been investigated. Again, the optimal coil phasing, predicted by the MARS-F code, is similar for the ITER scenarios with similar q_{95}. This implies that an optimally tuned ELM coil current waveform configuration at one current level should provide a reliable starting point for ELM control optimization at higher currents, provided that both the ELM coil current, plasma current and magnetic field are all proportionally scaled.

Optimization of toroidal torque profiles has been performed for the ITER scenario with 15 MA/5.3 T and fusion gain of Q=10. A strong coupling effect is generally observed between the core and edge torques, this coupling is due to the middle-row coil contribution, but somewhat weakened by inclusion of the upper and lower rows of coils and by the proper choice of the objective functions (e.g. OF3A). The solutions presented in table 3 thus may be used to refine the optimization of the current waveforms of the ELM control coils in further studies in preparation for ITER operation.

ACKNOWLEDGEMENTS

This work is funded by Fundamental Research Funds for the Central Universities. The work was also supported by the U.S. DoE Office of Science under Contract Nos. DE-FG02–95ER54309 and DEFC02–04ER54698. ITER is the Nuclear Facility INB no. 174. The views and opinions expressed herein do not necessarily reflect those of the ITER Organization.

REFERENCES

[1] Loarte A. et al., Nucl. Fusion 54 (2014) 033007.
[2] Evans T. et al., Phys. Rev. Lett. 92 (2004) 235003.
[3] Liang Y. et al., Phys. Rev. Lett. 98 (2007) 265004.
[4] Hawryluk R. J. et al., Nucl. Fusion 49 (2009) 065012.
[5] Kirk A. et al., Nucl. Fusion 50 (2010) 034008.
[6] Suttrop W. et al., Phys. Rev. Lett. 106 (2011) 225004.
[7] Jeon Y. M. et al., Phys. Rev. Lett. 109 (2012) 035004.
[8] Sun Y. et al., Phys. Rev. Lett. 117 (2016) 115001.
[9] Chapman I. T. et al., Plasma Phys. Control. Fusion 54 (2012) 105013.
[10] Evans T. E. et al., Nucl. Fusion 53 (2013) 093029.
[11] Orain F. et al., Phys. Plasmas 20 (2013) 102510.
[12] Nazikian R. et al., Phys. Rev. Lett. 114 (2015) 105002.
[13] Ryan D. A. et al., Plasma Phys. Control. Fusion 57 (2015) 095008.
[14] Liu Y. Q. et al., Nucl. Fusion 55 (2015) 063027.
[15] Li L. et al., Nucl. Fusion 56 (2016) 092008.
[16] Li L. et al., Plasma Phys. Control. Fusion 59 (2017) 044005.
[17] Liu Y. Q. et al., Phys. Plasmas 7 (2000) 3681.
[18] Wang Z. R. et al., Phys. Rev. Lett. 114 (2015) 145005.
[19] Liu Y. Q. et al., Nucl. Fusion 51 (2011) 083002.
[20] Liu Y. Q. et al., Nucl. Fusion 56 (2016) 066001.